Ann. Occup. Hyg., Vol. 56, No. 5, pp. 631–644, 2012

doi:10.1093/annhyg/mes006

Cytotoxicity and Genotoxicity of Nanosized and Microsized Titanium Dioxide and Iron Oxide Particles in Syrian Hamster Embryo Cells*

YVES GUICHARD[1]*, JULIEN SCHMIT[1], CHRISTIAN DARNE[1], LAURENT GATÉ[1], MICHÈLE GOUTET[1], DAVY ROUSSET[1], OLIVIER RASTOIX[1], RICHARD WROBEL[1], OLIVIER WITSCHGER[1], AURÉLIE MARTIN[1], VANESSA FIERRO[2] and STÉPHANE BINET[1]

[1]Institut National de Recherche et de Sécurité, Département Polluants et Santé, rue du Morvan, CS 60027, 54519 Vandoeuvre-Les-Nancy Cedex, France; [2]Institut Jean Lamour, Département 2: Chimie et Physique des Solides et des Surfaces, UMR 7198, CNRS—Nancy-Université—UPV-Metz, ENSTIB, 27 rue Philippe Séguin, BP 1041, 88051 Epinal cedex 9, France

Received 4 October 2011; in final form 12 December 2011; published online 26 March 2012

Potential differences in the toxicological properties of nanosized and non-nanosized particles have been notably pointed out for titanium dioxide (TiO_2) particles, which are currently widely produced and used in many industrial areas. Nanoparticles of the iron oxides magnetite (Fe_3O_4) and hematite (Fe_2O_3) also have many industrial applications but their toxicological properties are less documented than those of TiO_2. In the present study, the *in vitro* cytotoxicity and genotoxicity of commercially available nanosized and microsized anatase TiO_2, rutile TiO_2, Fe_3O_4, and Fe_2O_3 particles were compared in Syrian hamster embryo (SHE) cells. Samples were characterized for chemical composition, primary particle size, crystal phase, shape, and specific surface area. In acellular assays, TiO_2 and iron oxide particles were able to generate reactive oxygen species (ROS). At the same mass dose, all nanoparticles produced higher levels of ROS than their microsized counterparts. Measurement of particle size in the SHE culture medium showed that primary nanoparticles and microparticles are present in the form of micrometric agglomerates of highly poly-dispersed size. Uptake of primary particles and agglomerates by SHE exposed for 24 h was observed for all samples. TiO_2 samples were found to be more cytotoxic than iron oxide samples. Concerning primary size effects, anatase TiO_2, rutile TiO_2, and Fe_2O_3 nanoparticles induced higher cytotoxicity than their microsized counterparts after 72 h of exposure. Over this treatment time, anatase TiO_2 and Fe_2O_3 nanoparticles also produced more intracellular ROS compared to the microsized particles. However, similar levels of DNA damage were observed in the comet assay after 24 h of exposure to anatase nanoparticles and microparticles. Rutile microparticles were found to induce more DNA damage than the nanosized particles. However, no significant increase in DNA damage was detected from nanosized and microsized iron oxides. None of the samples tested showed significant induction of micronuclei formation after 24 h of exposure. In agreement with previous size-comparison studies, we suggest that *in vitro* cytotoxicity and genotoxicity induced by metal oxide nanoparticles are not always higher than those induced by their bulk counterparts.

Keywords: agglomeration; comet assay; cytotoxicity and genotoxicity of titanium dioxide and iron oxide; micronucleus assay; nanoparticles and microparticles; particle characterization; particle uptake; reactive oxygen species; relative increase cell count; Syrian hamster embryo cells

*Author to whom correspondence should be addressed. Tel: +33-383-508-503; fax: +33-383-502-096;
e-mail: yves.guichard@inrs.fr
* *based on presentations at the INRS Symposium on Risks of Nanoparticles and Nanomaterials, Nancy, France, April 2011.*

INTRODUCTION

Nanoparticles, defined as particles having at least one dimension <100 nm (EC, 2011), possess physical and chemical properties that are generally not found in non-nanoscale particles of the same chemical composition. The diversity of engineered nanoparticles in chemical composition, size and shape, and the lack of exposure data have given rise to concern about their impact on human health, making their regulation difficult (Savolainen *et al.*, 2010). In particular, the question of whether the toxicological effects of nanoparticles are fundamentally different from those shown by larger particles of identical composition has not yet been elucidated (Auffan *et al.*, 2009a). Differences in the toxicological properties of nanoscale and microscale particles have been notably pointed out for titanium dioxide (TiO_2) particles. Engineered TiO_2 particles are currently widely produced and used in many industrial areas, including paints, plastics, food colorants, and cosmetics. Fine TiO_2 particles (or those of undefined size) have long been considered poorly toxic. However, recent *in vivo* studies focusing on particles of nanoscale size have demonstrated that TiO_2 can cause inflammatory responses in the airways of rats and mice and fibrosis or lung tumors in rats (Bermudez *et al.*, 2004; Warheit *et al.*, 2007). Based on these data, TiO_2 has been classified by The International Agency for Research of Cancer as possibly carcinogenic to human (Group 2B) (IARC, 2010). In addition, a number of *in vitro* studies have shown the capacity of TiO2 nanoparticles to induce cytotoxicity, reactive oxygen species (ROS), and genotoxicity in various cell lines (Gurr *et al.*, 2005; Wang *et al.*, 2007; Bhattacharya *et al.*, 2009; Falck *et al.*, 2009).

Few studies have directly compared the toxicological effects of engineered nanoscale and microscale TiO_2 particles. Instillation studies in rats and mice indicate stronger toxicological effects from nanosized TiO_2 compared to fine TiO_2 (Oberdorster *et al.*, 1990, 1992). Similarly, nanosized TiO_2 has been shown to induce more cytotoxic and genotoxic effects (DNA damage and micronucleus induction) in cultivated cells than fine TiO_2 (Rahman *et al.*, 2002; Gurr *et al.*, 2005). These results have been explained by the higher specific surface area (SSA) of nanoparticles compared to larger particles, which may enhance, for a given mass, intracellular ROS production (Oberdorster *et al.*, 2005). However, the effects of nanosized TiO_2 are not always enhanced when compared to their bulk counterparts. An instillation study in rats using TiO_2 particles of various sizes showed that the inflammatory effects induced by nanosized particles were no more potent than those of larger particles (Warheit *et al.*, 2007). Moreover, microsized particles of TiO_2 induced *in vitro* more DNA damage than TiO_2 nanoparticles (Falck *et al.*, 2009; Karlsson *et al.*, 2009). These apparently conflicting results might be explained not only by the diversity of the experimental models employed but also by the origin of TiO_2 particles used for comparison. Due to industrial processes, engineered nanoscale and microscale TiO_2 particles of the same chemical composition do not necessarily have the same physicochemical structure (Schulze Isfort and Rochnia, 2009). In particular, engineered TiO_2 particles exist in three different crystal structure forms: anatase, rutile, and brookite (IARC, 2010). In the size-comparison studies above, nanoscale and microscale TiO_2 particles were not always of the same crystal structure and varied also in shape or surface coating.

Like TiO_2, nanoparticles of the iron oxides magnetite (Fe_3O_4) and hematite (Fe_2O_3) have many industrial applications, including environmental catalysis, magnetic storage, biomedical imaging, and magnetic target drug deliver (Hood, 2004), but their toxicity is less documented. *In vivo* and *in vitro* studies suggest that Fe_3O_4 nanoparticles have a low toxic potential (Hussain *et al.*, 2005; Jeng and Swanson, 2006; Karlsson *et al.*, 2009; Liu *et al.*, 2009). Fe_2O_3 nanoparticles, however, have been shown to induce lung inflammation in mice (Zhu *et al.*, 2008) as well as *in vitro* cytotoxic effects (Soto *et al.*, 2007). One *in vitro* study reported no clear difference between nanosized and microsized Fe_3O_4 and Fe_2O_3 particles in their capacity to induce DNA damage (Karlsson *et al.*, 2009).

The difference in toxicity between engineered TiO_2 and iron oxide nanoparticles and their bulk counterparts is unclear, but it is possible that the reduction in particle size also involves structural change. The aim of the present study was therefore to compare the *in vitro* cytotoxicity and genotoxicity of chemically and physically well-characterized nanosized and microsized anatase TiO_2 and rutile TiO_2, Fe_3O_4, and Fe_2O_3 particles in Syrian hamster embryo (SHE) cells. This cell type has previously been used to demonstrate the induction of micronuclei by ultrafine TIO_2 (Rahman *et al.*, 2002).

MATERIALS AND METHODS

Particle source

Nanoparticles and microparticles of anatase TiO_2, rutile TiO_2, Fe_3O_4, and Fe_2O_3 were purchased

Table 1. Chemical and physical particle characterization.

Name	Description[a]	Chemical impurity (%)[b]	Particle size[c] (nm)	BET SSA (m^2 g^{-1})[d]
TiO_2 A nano	Titanium (IV) oxide, anatase, and nanopowder; Sigma 637254	<0.5	14 ± 4	149
TiO_2 A micro	Titanium (IV) oxide, anatase, and powder; Sigma 232033	<0.5	160 ± 48	9
TiO_2 R nano	Titanium (IV) oxide, rutile, and nanopowder; Sigma 637262	11% SiO_2, 1% Na_2O, and 1% SO_4	62 ± 24 × 10 ± 2	177
TiO_2 R micro	Titanium (IV) oxide, rutile, and powder; Sigma 224227	<0.5	530 ± 216	3
TiO_2 P25	Aeroxide® TiO_2 P25; ∼80% anatase; ∼20% rutile; Evonik-Degussa	<0.5	25 ± 6	58
Fe_3O_4 nano	Iron (II,III) oxide and nanopowder; Sigma 637106	<0.5	27 ± 8	40
Fe_3O_4 micro	Iron (II,III) oxide and powder; Sigma 310069	<0.5	156 ± 82	7
Fe_2O_3 nano	Iron (III) oxide and nanopowder; Sigma 544884	<0.5	35 ± 14	39
Fe_2O_3 micro	Iron (III) oxide and powder; Sigma 310050	<0.5	147 ± 48	6

[a]According to the supplier.
[b]Impurities in Si, Mg, Al, Cr, K, Na, Ca, Ta, Mn, Ni, Zn, Cd, Nb, and Mo were determined by ICP–AES. Only Si impurities were examined in micro rutile TiO_2.
[c]Values represent the mean ± SD particle diameter (rod length for TiO_2 R nano) measured by TEM in 100 particles.
[d]SSA as determined by the Brunauer, Emmett, and Teller calculation method.

from Sigma-Aldrich (France). TiO_2 P25 was donated by Evonik-Degussa (Germany). Supplier descriptions are given in Table 1. Sample powders were used as received, and no further modifications were applied.

Chemical composition and crystal phase

TiO_2 samples were mineralized by acid digestion in HF and Na_2CO_3 alkaline melting. Iron oxide samples were mineralized by acid digestion in an HCl–HNO_3 mixture. Nano-Fe_2O_3 was also mineralized by acid digestion in HF for the determination of Si and Na contents. Concentrations of major elements (Ti and Fe) and impurities (Si, Mg, Al, Cr, K, Na, Ca, Ta, Mn, Ni, Zn, Cd, Nb, and Mo) were determined by inductively coupled plasma and atomic emission spectrometry (ICP–AES, Spectro Ciros, Germany). The degree of crystallinity of all samples was determined by X-ray diffraction using a X'Pert diffractometer (Panalytical, The Netherlands).

Primary particle size

Primary particle size was determined by transmission electronic microscopy (TEM). Particle powders suspended in isopropanol were loaded onto TEM grids under vacuum and observed with a 100 kV Zeiss EM 910 TEM (Zeiss, Germany), equipped with a ProgRes CF Scan (Jenoptik, Germany) camera. Determinations of primary particle size distribution were based on 100 measurements of particles from ×100 000 magnified TEM images. Particle diameter was calculated using free image processing software (ImageJ, National Institute of Health, USA), assuming spherical primary particle form.

SSA and solid density

N2 adsorption–desorption isotherms were obtained at 77K using Micromeritics ASAP 2020 automatic apparatus (Micromeritics, France). Samples were degassed under vacuum at 473K for 10 h prior to adsorption experiments. N2 adsorption data were obtained by dosing N2 at relative pressures between 10-3 and 0.99. SSAs were determined using the Brunauer, Emmett, and Teller (BET) calculation method (Brunauer *et al.*, 1938).

Particle size in culture medium

Particle size in the SHE culture medium was assessed by dynamic light scattering (DLS) and laser diffraction (LD) techniques. The DLS instrument was a VASCO-2 particle-size analyser (Cordouan Technologies, France). Particle size was determined using the light-scattering intensity-averaged or Z-averaged diameter (dZ), obtained from analysis of the autocorrelation function by the cumulants method (ISO, 2008). LD particle size analyses were performed with a Mastersizer® X (Malvern Instruments, Worcestershire, UK). All LD data were evaluated by volume distribution. The median volume diameter was calculated (= 50% volume percentile, d50,V), as well as the volume diameters at 10% (d10,V) and 90% (d90,V), respectively. The number distribution was derived from the volume distribution assuming a spherical model for the particles. For DLS and LD

measurements, particles were suspended in the SHE culture medium at 1 mg ml^{-1} to form the stock solution and then sonicated for 20 min at 40 Watt using a sonicator bath (Brandson B-8510, France). Particle suspensions were then diluted in the culture medium at 43.75 μg ml^{-1}, which is within the range of the concentrations used in cellular assays (25 μg of particles per cm^2 of culture surface).

Acellular ROS assay

Intrinsic ROS production from particles was assessed as previously described (Cohn *et al.*, 2008). This method uses the 3′-(p-aminophenyl)fluorescein (APF) molecule (Invitrogen, France), which becomes fluorescent in the presence of various ROS, mainly hydroxyl radicals, peroxynitrite anions, and hypochlorite anions (Setsukinai *et al.*, 2003). Particles were suspended in 50 mM potassium phosphate buffer (Sigma-Aldrich) at 1 mg ml^{-1} and sonicated according to the procedure described above. Dilutions of particle suspensions (250 μg ml^{-1}) and APF (10 μM) in the phosphate buffer, with and without H_2O_2 (80 mM Sigma-Aldrich), were incubated under agitation for 18 h at room temperature. After incubation, particle suspensions were centrifuged at 17 000 g for 5 min at room temperature. Supernatant fluorescence was measured using a Synergy HT (Biotek®, France) plate reader with excitation and emission wavelengths set to 490 and 520 nm, respectively. To avoid possible photocatalytic activity of anatase TiO_2 (Sclafani and Herrmann, 1996), assays were protected from direct light exposure.

Cell culture and particle treatment

SHE cell cultures were established from individual 13-day gestation fetuses (inbred colony, INRS, France) (Pant and Aardema, 2008). Secondary cultures were used in the study. Cells were cultured at 37°C, 10% CO_2, in Dulbecco's modified Eagle's medium (Invitrogen, France), supplemented with 20% fetal bovine serum (Hyclone, France) and antibiotics (50 units ml^{-1} Penicillin, 50 μg ml^{-1} Steptomycin; Invitrogen). At 80% confluence, cells were harvested using 0.25% trypsin and 0.53 mM ethylenediaminetetraacetic acid (EDTA) and were sub-cultured into a culture support appropriate for the type of experiment selected. Cells were allowed to attach to the surface for 24 h prior to treatment. Under such conditions, the doubling time of cell cultures was ∼18 h. On the day of treatment (at ∼50% cell confluence), particles were suspended in culture medium at 1 mg ml^{-1} and sonicated according the procedure describe above. Appropriate serial dilutions of particle suspensions, thoroughly mixed each time, were added to the cell cultures. Nanoparticles and microparticles of the same chemical composition were tested in the same experiment. All cellular assays were protected from direct light exposure.

Cellular uptake assay

Cells were cultured on Thermanox™ coverslips (Nunc, Thermofisher, France) and treated with particles (1 μg cm^{-2}) for 24 h. After treatment, cells were fixed in glutaraldehyde 2% (Sigma, St Louis, MO, USA) in phosphate buffer saline (PBS; Invitrogen, France) before washing in PBS and distilled water. The samples were post-fixed in 1% OsO4 in water before classical processing for Araldite embedding and ultramicrotomy. The ultrathin sections were counterstained with uranyl acetate and observed with a Hitachi 7500 transmission electron microscope (Hitachi High Technologies Corporation, Tokyo, Japan) equipped with an AMT Hamamatsu digital camera (Hamamatsu Photonics, Hamamatsu City, Japan).

Cytotoxicity assay

Cell cultures in 12-well plates were treated with particles at concentrations between 0.5 and 200 μg cm^{-2} for 24 and 72 h. After treatment, cells were removed by trypsination and counted using an automated counter (Coulter Z1, Beckman Coulter, France). Evaluation of the cytotoxicity was based on the relative cell count (RCC). EC50 values (particle concentrations) at 50% RCC were calculated from curves representing RCC change after 72 h of exposure with respect to particle concentration.

$$\mathrm{RCC} = \frac{\text{number of cells in treated cultures}}{\text{number of cells in control cultures}} \times 100.$$

Intracellular ROS assay

The 2′,7′-dichlorofluorescein diacetate (DCFDA) non-fluorescent is capable of passively entering a cell at the location where cellular esterases hydrolyze its acetyl moieties. The probe is susceptible to reaction with a variety of ROS, including hydrogen peroxide, peroxyl radicals, and peroxynitrite anions, to form the highly fluorescent dichlorofluorescein (LeBel *et al.*, 1992). Cell cultures in 12-well plates were treated with particles (1, 5, and 10 μg cm^{-2}) for 72 h. After treatment, the culture medium was removed and cells were incubated for 30 min at 37°C with 25 μM DCFDA (Invitrogen) pre-diluted in Hank's Balanced Salt Solution (HBSS) (Invitrogen, France). At the end of incubation, cells were recovered by trypsination. Propidium iodide (Sigma-Aldricht)

was added to the cell suspensions (50 μg ml^{-1}) and fluorescence intensity within live cells (at least 20 000 cells) was immediately measured using a flow cytometer (FACStarPLUS-Becton Dickinson, France). Intracellular ROS content was expressed by the fold change of the mean fluorescence intensity in exposed cells with respect to the control.

Comet assay

The comet assay was performed as previously described (Collins *et al.*, 1998). Cell cultures in 21-cm^2 dishes were treated with particles (10, 25, and 50 μg cm^{-2}) for 24 h. Sets of TiO_2 particles and iron oxides particles were tested separately. Methyl methanesulfonate (MMS, Sigma-Aldrich) treatment at 0.5 mM was used as a positive control. After treatment, cells were harvested by trypsination and were resuspended in 600 μl of molten (37°C) 0.5% low melting agarose (Sigma-Aldrich). Aliquots of cell–agarose mixtures (100 μl) were loaded onto a slide pre-coated with 1% normal melting agarose (Sigma-Aldrich). Slides were immersed in cold lysis solution (2.5 M NaCl, 100 mM Na_2EDTA, 10 mM Tris with 1% Triton X-100, and 10% DMSO) for 1 h at 4°C. Slides were then drained and immersed in cold alkaline solution (300 mM NaOH, 1mM Na_2EDTA; pH 13) for 20 min. Electrophoresis was performed in the same buffer at 25 V and 300 mA for 40 min. The slides were then washed with Tris–HCl 0.4 M for 15 min and DNA was stained with propidium iodide (2.5 μg ml^{-1}) for 1 h. Comet analysis was performed using a fluorescence microscope coupled with image analyzer software (Comet Assay IV; Perceptive Instruments, UK). For each sample, the mean percentage of DNA in the comet tail was determined in 100 cells per slide as a measure of DNA damage.

Micronucleus assay

Cell cultures in Labtek® slides (Nunc, Thermofisher, France) were treated with particles (5, 10, and 50 μg cm^{-2}) for 24 h. MMS treatment at 0.1 mM was used as a positive control. After treatment, cells were washed with PBS and fixed in methanol for 20 min. DNA was stained with DAPI (Pro Long Gold antifade reagent®, Invitrogen, France). Around 1000 cells per slide were analyzed using a fluorescence microscope. Micronucleated cells (containing at least one micronucleus) were scored. The effect of treatment on cell division was evaluated on the basis of the relative increase in cell count (RICC) (OECD, 2010), calculated from data obtained in the cytotoxicity assays.

Statistics

Each experiment was performed at least three times and experimental data are given as a mean ± standard deviation (mean ± SD). The statistical significance of differences between control and treated groups and between nanoparticle and microparticle groups in each assay was subjected to a Student *t*-test (two sides) based on assumed equal variance, except for intracellular ROS assays where statistical analysis was performed by one-way analysis of variance and Dunnett's test. Differences between groups were considered significant when $P < 0.05$.

RESULTS

Particle characterization

A summary of the particle characterizations is given in Table 1. Chemical impurities were lower than 0.5%, except for the rutile TiO_2 nanoparticles, which contained SiO_2 (11%), Na_2O (1%), and SO_4 (1%). Qualitative analysis of the crystal phase indicated that the TiO_2 samples labeled anatase and rutile by the supplier contained some traces of rutile and anatase, respectively. The TiO_2 P25 contained both crystal phases as indicated in the supplier's description. As expected for the iron oxide samples, the main crystal phases were magnetite for Fe_3O_4 particles and hematite (Fe_2O_3-alpha) for Fe_2O_3 particles. However, the presence of magnetite, hematite, and maghemite (Fe_2O_3-gamma) was detected in all iron oxide particles. TEM micrographs of nanoparticle and microparticle powders showed predominantly particle agglomerates (not shown). All primary nanoparticles and microparticles had a spherical shape, except for rutile TiO_2 nanoparticles, which were observed as rods. Individual nanoparticle sizes determined by TEM ranged from 14 to 35 nm. The primary sizes of particles labeled microparticles were in the sub-micrometric scale, ranging from 147 to 530 nm.

$$\mathrm{RICC} = \frac{\text{increase in number of cells in treated cultures (end of treatmnet } - \text{ initial seeding)}}{\text{increase in number of cells in control cultures (end of treatmnet } - \text{ initial seeding)}} \times 100.$$

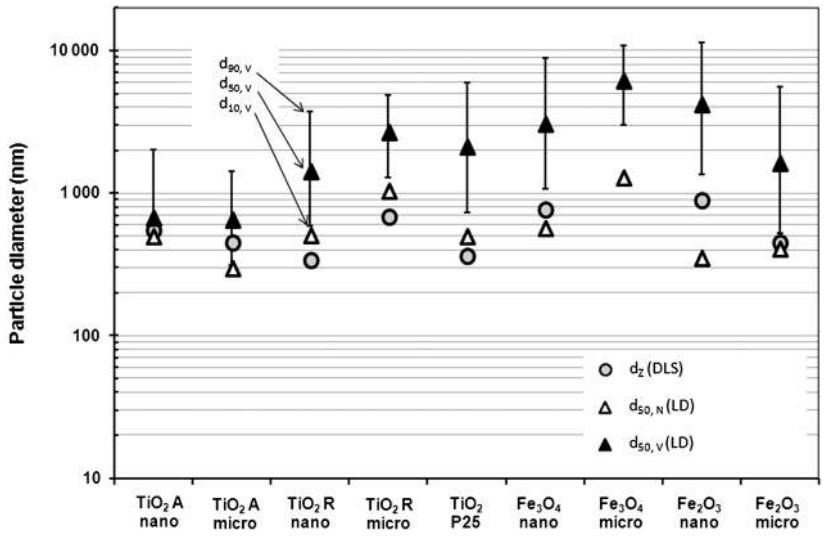

Fig. 1. Z-average hydrodynamic diameter (dZ) measured by DLS and number (d50,N) and volume (d50,V) median diameters measured by LD for the different types of nanoparticles and microparticles suspended in the SHE culture medium (43.75 μg ml^{-1}). Each diameter value corresponds to an average of three replicates. Standard deviation intervals are not shown for the sake of clarity. The lower and upper limits of the bars correspond to the volume diameters at 10% (d10,V) and 90% (d90,V), respectively.

SSA, as evaluated by the BET method, was higher for nanoparticle samples (39–177 m^2 g^{-1}) than for microparticle samples (3–9 m^2 g^{-1}).

Particle size in the culture medium

Diameters measured by DLS or LD techniques suggest that all particle suspensions in the SHE culture medium consisted of mainly agglomerated particles (Fig. 1). Particle diameters determined by DLS (dZ) varied from ∼300 to 700 nm depending on the particle type. The coarse particles present in the suspension of Fe_3O_4 microparticles made the determination of dZ impossible for this sample. With the exception of Fe_2O_3 nanoparticle suspensions, the d50, *N* values measured by LD were close to the dZ values. However, LD results expressed by volume (d90,V; d50,V; and d10,V) reveal a broad range of size distributions for all particle suspensions. Taken together, the DLS and LD results indicate that suspension of anatase TiO_2 nanoparticles led to coarser particle formation than its microsized counterpart. The contrary was observed for rutile TiO_2. Among the iron oxide samples, the particle population of the nano-form Fe_3O_4 was finer than the micron-form, while the opposite was observed for Fe_2O_3 samples.

ROS generation in acellular condition

In the absence of H_2O_2, a significant increase in fluorescence was observed for all TiO_2 particles but not for iron oxides (Fig. 2). Anatase TiO_2 nanoparticles and TiO_2 P25 particles produced the highest level of ROS. ROS activity was found to be significantly stronger for the anatase and rutile nanoparticles than for their micrometer counterparts. The ROS activity of Fe_3O_4 and Fe_2O_3 was detected when particles were incubated in the presence of H_2O_2, with a higher intensity for the nanoparticles than for microparticles.

Particle uptake by SHE

TEM analysis of SHE cultures exposed to particles indicated that all TiO_2 and iron oxide nanoparticles or microparticles are able to penetrate cells in the form of individual particles and agglomerates. As an example, Fig. 3 shows TiO_2 P25 uptake in an SHE cell after 24 h of exposure to particles at 1 μg cm^{-2}.

Cytotoxic effect

Independent of particle size, RCC decreases were higher for TiO_2 particles than for iron oxide particles after 24 or 72 h of exposure (Fig. 4). The differences in cytotoxicity for all particle types were more pronounced after 72 h than after 24 h of exposure. After 72 h, the EC50 values obtained with anatase and rutile TiO_2 nanoparticles and TiO_2 P25 were in the same range (∼10 μg cm^{-2}) (Table 2). When comparing the EC50 values obtained at 72 h for nanoparticles and microparticles of the same chemical

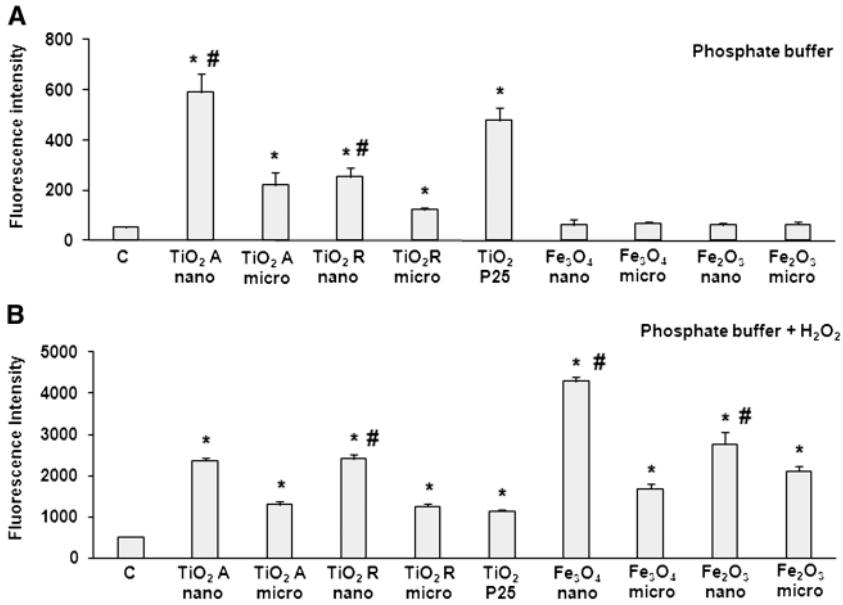

Fig. 2. ROS production induced by nanoparticles and microparticles in acellar assays. Particles (250 μg ml^{-1}) were incubated with APF (10 μM) for 18 h in (A) phosphate buffer and (B) phosphate buffer containing H_2O_2 (80 mM). After centrifugation, fluorescence in supernatants was measured at 490 nm excitation and 520 nm emission wavelengths. Each bar represents the mean ± SD of values obtained in three assays. *Significantly different from control (C); #significant difference between nanoparticles and microparticles ($P < 0.05$).

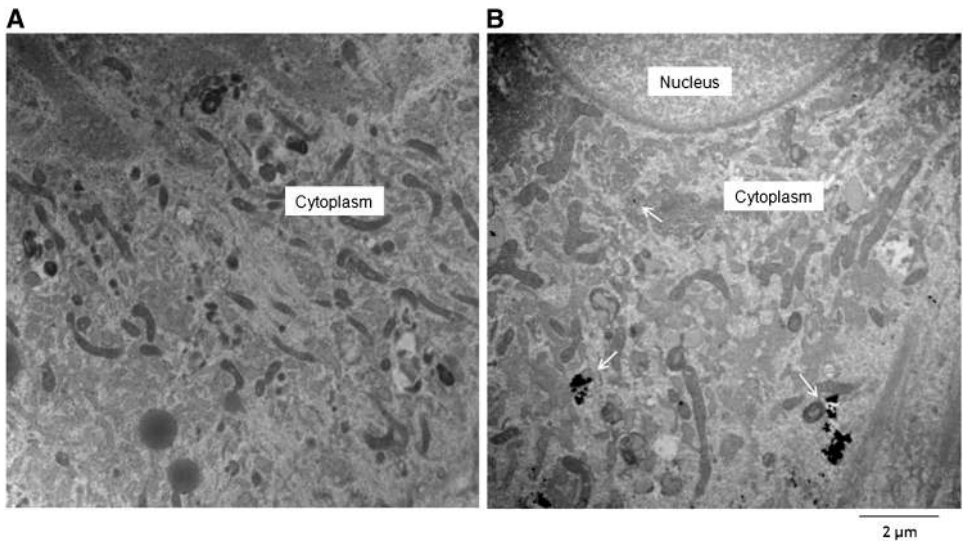

Fig. 3. TEM—image of (A) unexposed cells and (B) cells exposed to TiO_2 P25 for 24 h. Arrows indicate examples of isolated nanoparticles and agglomerates observed in the cytoplasm.

composition, anatase TiO_2, rutile TiO_2, and Fe_2O_3 nanoparticles were significantly more cytotoxic than their micrometer counterparts (∼3-fold, 2-fold, and >3-fold, respectively). No difference was observed between Fe_3O_4 nanoparticles and microparticles.

Intracellular ROS production

An increase in ROS was detected after 24 h of exposure to all TiO_2 samples. In the case of the iron oxides, only Fe_2O_3 nanoparticle exposure resulted in an ROS increase (Fig. 5). Anatase TiO_2 nanoparticles

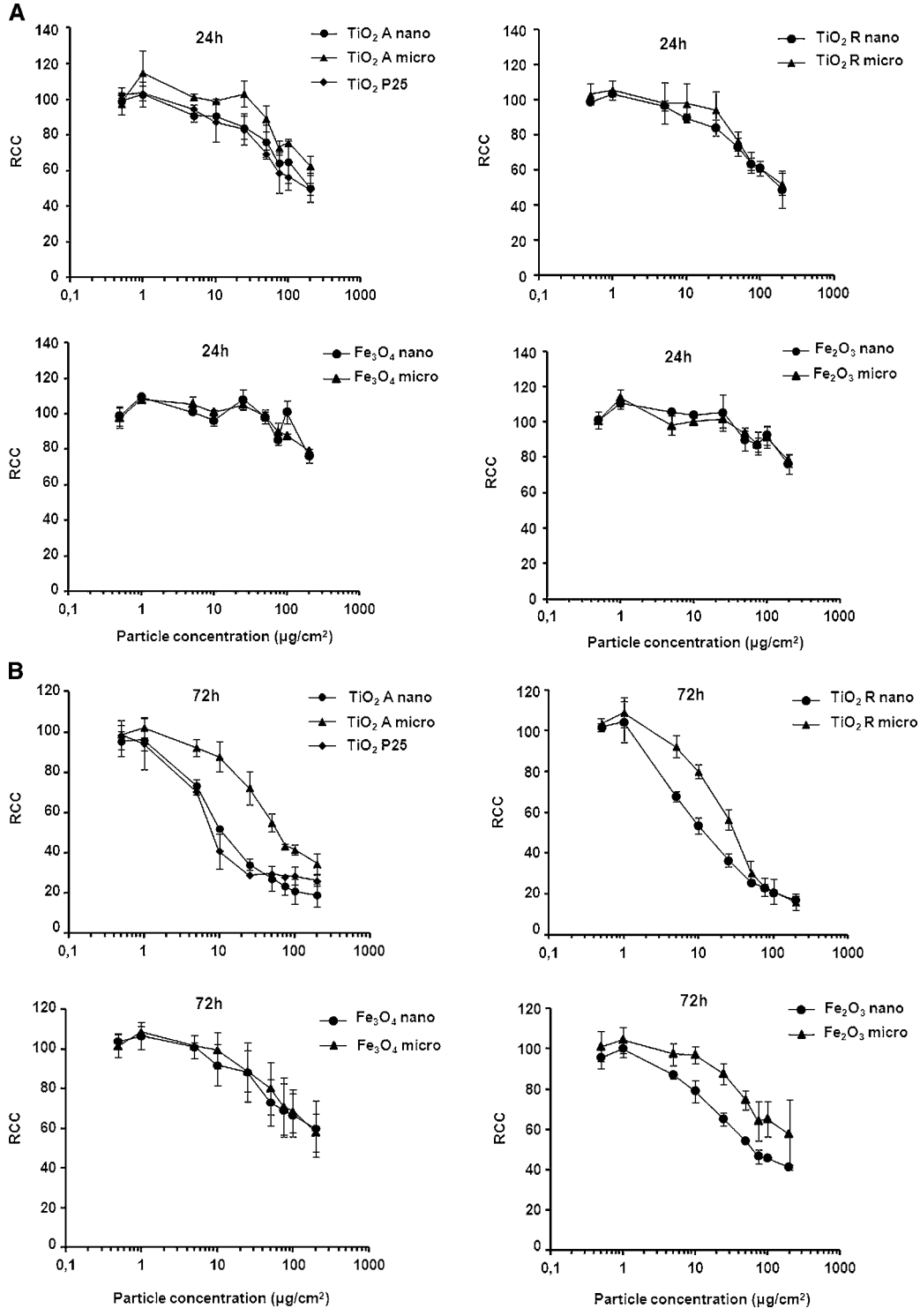

Fig. 4. Dose–response of cytotoxicity (RCC decrease) in SHE exposed to 0.5, 1, 5, 10, 50, 75, 100, and 200 µg cm^{-2} nanoparticles and microparticles for (A) 24 h and (B) 72 h. Each point represents the mean ± SD RCC obtained in three independent experiments.

induced the highest ROS increase compared to the other particles. At 10 μg cm^{-2}, the increase in ROS was significantly higher for anatase TiO_2 and Fe_2O_3 nanoparticles than for their micrometer counterparts.

DNA damage

At the highest particle concentration (50 μg cm^{-2}), all TiO_2 particles except rutile nanoparticles caused increased DNA damage after 24 h of exposure. In contrast, no significant DNA damage was found with iron oxide particles, whatever the concentration tested (Fig. 6). TiO_2 P25 was the only particle that induced a significant effect at all concentrations. The highest levels of DNA damage were obtained with anatase TiO_2, with no significant difference between nanoparticles and microparticles. In contrast, rutile TiO_2 microparticles induced significant DNA damage at the highest concentration, whereas rutile TiO_2 nanoparticles did not. The positive assay control (MMS at 0.5 mM) induced significant DNA damage in SHE cells.

Table 2. EC50 values obtained from RCC curves acquired after 72 h of exposure.

Particles	EC50
TiO_2 A nano	12.0 ± 0.2
TiO_2 A micro	59.2 ± 6.1
TiO_2 R nano	15.2 ± 4.3
TiO_2 R micro	30.7 ± 6.1
TiO_2 P25	9.6 ± 1.3
Fe_3O_4 nano	ND
Fe_3O_4 micro	ND
Fe_2O_3 nano	65.1 ± 4.8
Fe_2O_3 micro	ND

ND, not determinable.

Micronucleus formation

No significant micronucleus formation was detected in SHE exposed to particles (5, 10, and 50 μg cm^{-2}) for 24 h (Fig. 7). All particle concentrations used in the assay induced a decrease in RICC of <50%. The decreases in micronucleus frequency observed at the highest concentration of TiO_2 particles (50 μg cm^{-2}) when compared to the control may be explained either by some blockage to division induced by the treatment or by the presence of particles on the slide which disturbed micronucleus scoring. The positive assay control (0.1 mM MMS) significantly increased the number of micronucleated cells with inducing a decrease in RICC of ∼20%.

DISCUSSION

In this size–effect comparison study, we used commercially available TiO_2 and iron oxide nanoparticles and microparticles of the same chemical composition. TiO_2 P25, which has been used in several toxicological studies, was also included in our assay as a reference nanoparticle. With the exception of the rutile TiO_2 nanoparticles, no significant chemical impurities were detected in any samples. This sample, which was described by the supplier as 99.5% pure, contained a non-negligible amount of SiO_2, which may correspond to a nanoparticle coating material. Qualitative crystallographic analyses indicated that none of the samples can be considered to be completely pure in their crystal phase. The mixture of different crystal phases in iron oxide

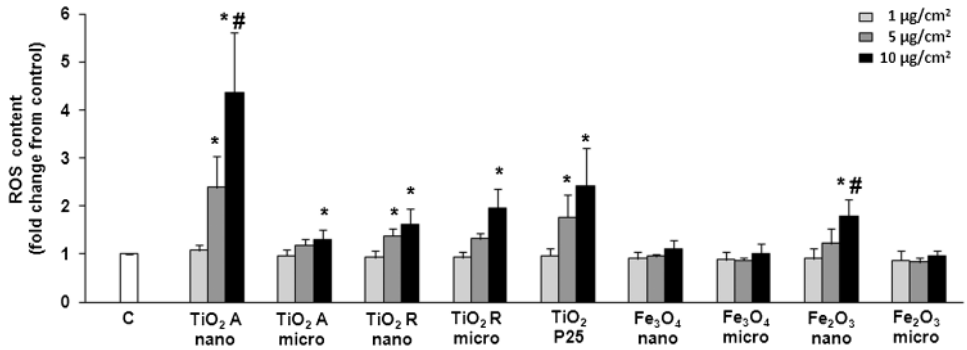

Fig. 5. Intracellular ROS content in SHE exposed to 1, 5, and 10 μg cm^{-2} nanoparticles and microparticles for 72 h. Dichlorofluorescein fluorescence within at least 20 000 live cells was detected by flow cytometry. Each bar represents the mean ± SD of values obtained in three independent experiments. *Significantly different from control (C); #significant difference between nanoparticles and microparticles ($P < 0.05$).

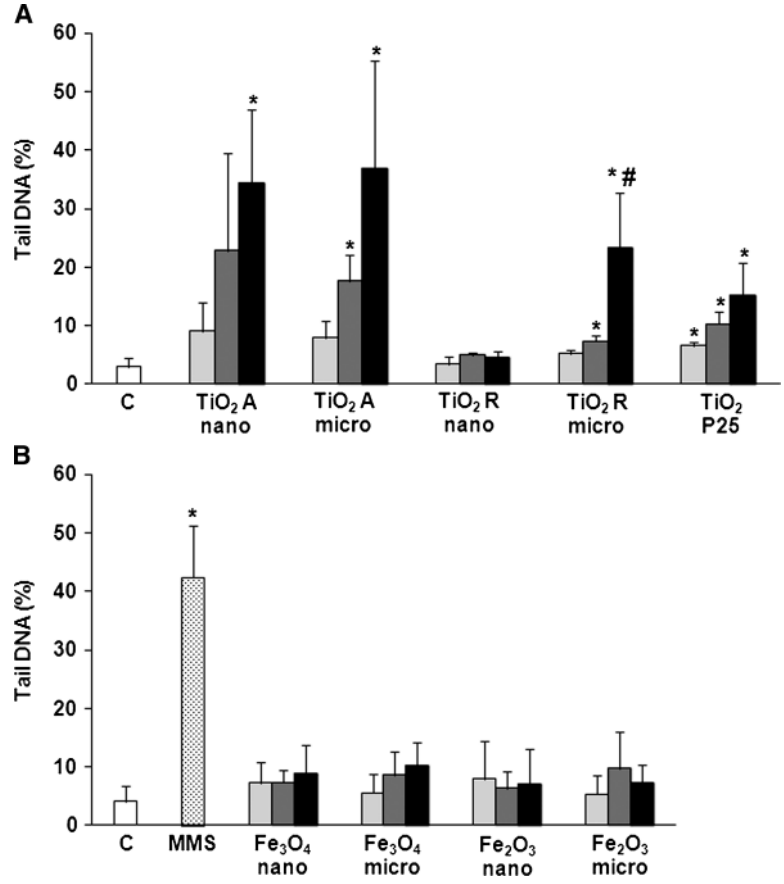

Fig. 6. DNA damage in SHE exposed to 10, 25, and 50 μg cm^{-2} TiO_2 (A) and iron oxide (B) nanoparticles and microparticles for 24 h. The mean percentage of DNA in the tail was determined in 100 cells. Each bar represents the mean ± SD of values obtained in three independent experiments. *Significantly different from control (C); #significant difference between nanoparticles and microparticles ($P < 0.05$).

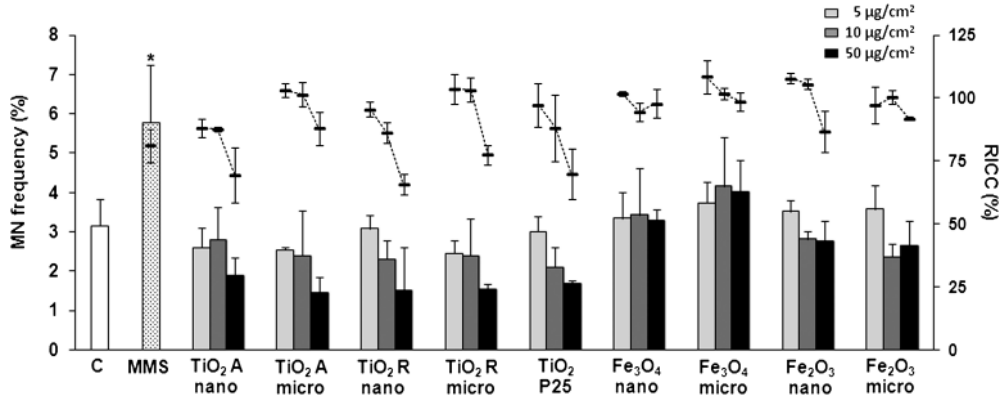

Fig. 7. Micronucleus formation in SHE exposed to 5, 10, and 50 μg cm^{-2} nanoparticles and microparticles for 24 h. Micronucleated cells were scored in at least 1000 cells. Each bar represents the mean ± SD of values obtained in three independent experiments. RICC was calculated from data obtained in the cytotoxicity assays. *Significantly different from control (C) ($P < 0.05$).

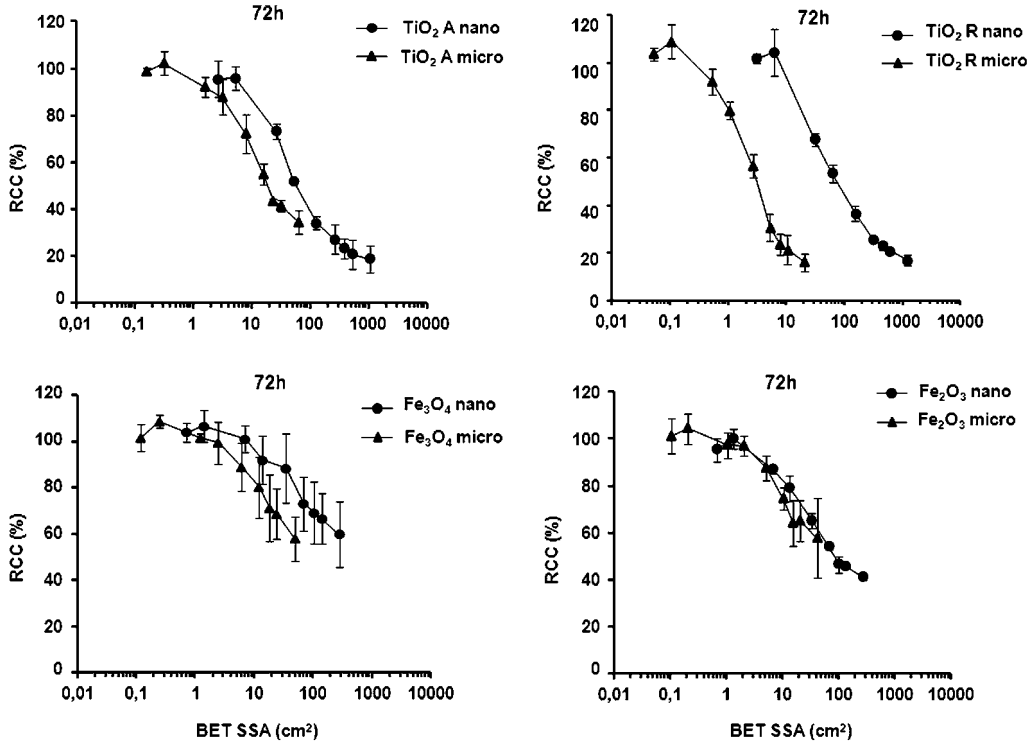

Fig. 8. Dose–response of cytotoxicity (RCC decrease) induced by nanoparticles and microparticles with dose expressed as BET SSA.

samples was possibly a consequence of their chemical instability (Auffan *et al.*, 2009b). In the case of TiO_2 samples, a unique crystal phase of anatase or rutile is probably difficult to achieve by industrial processes. With regard to particle size and surface, all samples labeled as nanoparticles by the supplier were in agreement with the definition of a nanomaterial ($<$100 nm at least one dimension) and had a BET SSA higher than those of microparticle samples. However, samples named as microparticles were rather in the sub-micrometric range ($>$100 nm and $<$1 μm).

The initial state of powder samples was in the form of micrometer aggregates or agglomerates. As already shown in several studies, agglomerate size in a culture medium could be influenced by the dispersion procedure (Allouni *et al.*, 2009; Kato *et al.*, 2009). In the present study, particle suspensions were homogenized by sonication without trying to reduce the size of agglomerates, assuming that coarse particles could also be present in a putative situation of human exposure. Agglomerate size was assessed by a combination of DLS and LD measurements. The LD technique has a wide detection range and is able to characterize particles both in the submicron- and in the micron-sized range. Results revealed that all sample suspensions were composed of agglomerates of highly poly-dispersed size, with the presence of coarse microsized agglomerates. The general trend of agglomerate size change between the nanosized and microsized primary particles was not the same for all metal oxides examined.

The intrinsic free radical activity of particles was also an element of particle characterization. The generation of free radicals on the surfaces of TiO_2 particles is explained by discontinuities and/or defaults in the crystal structure. The anatase phase was previously shown to generate higher levels of free radicals than the rutile phase (Arenz *et al.*, 2005; Fenoglio *et al.*, 2009). Iron oxide particles are known to behave like transition metals (Fe^{2+} and Fe^{3+}), which are able to produce oxygenated free radicals through a Fenton-like reaction with intermediate molecules, such as H_2O_2 (Auffan *et al.*, 2009b). In solution, active sites of TiO_2 and iron oxide particles can react with water or oxygen to generate various ROS, including superoxide anions, hydroxyl radicals, and singlet oxygen. In the absence of H_2O_2, ROS production was detected for all TiO_2

particles, the anatase phase being more active than the rutile phase but not for the iron oxide particles. However, the presence of H_2O_2 in the reaction mixture triggered an ROS activity signal for all iron oxide particles. In a previous study, in which ROS activity was assessed by electron paramagnetic resonance, Fe_2O_3 nanoparticles (and not TiO_2) needed additional intermediate molecules (H_2O_2 and ascorbic acid) to generate radicals (Bhattacharya *et al.*, 2009). For both TiO_2 and iron oxides, the level of ROS activity generated by nanoparticles was higher in magnitude compared to their micrometer counterparts at the same mass dose.

Regarding toxicological issues, observed particle uptake by SHE after 24 h of exposure did not seem to depend on chemical composition, primary size, nor the size of agglomerates. Based on measured RCC decreases, TiO_2 induced more cytotoxicity than iron oxides whatever the primary size of particles. When focusing on the primary size–effects for particles of the same chemical compositions and at the same mass dose, anatase and rutile TiO_2 and Fe_2O_3 nanoparticles induced higher cytotoxic effects than their micrometer counterparts after 72 h of exposure. The absence of observed size–effects for Fe_3O_4 may be explained by the low cytotoxity induced by both nanoparticles and microparticles. When expressed per unit of BET SSA (Fig. 8), the cytotoxicity of nanoparticles and microparticles of the same composition cannot be directly correlated to their BET SSA and microparticles might be considered to be more cytotoxic than nanoparticles, with the exception of Fe_2O_3. However, with regard to particle agglomeration in the culture medium, results should be interpreted carefully because the BET SSA may be not representative of the biologically active surface. Referring to Fig. 1, no clear relationship between agglomerate size and cytotoxic effects can be identified. Results may also reflect variation in surface reactivity between nanosized and microsized particles, possibly due to differences in crystallinity or/and coating in the case of rutile TiO_2.

Previously published data show that the cytotoxic effect of TiO_2 and iron oxide nanoparticles depends on the cell type used, the cytotoxic endpoint considered, and the origin of the manufactured samples. Some studies have compared the cytotoxic effects of nanoparticles and microparticles. In a human alveolar epithelial cell line (A549) exposed for 24 h, a higher cytotoxic effect was observed for 30–60 nm than for 0.5–1 μm Fe_2O_3 particles but no differences were observed between 20–40 nm and 0.1–0.5 μm Fe_3O_4 or between 20–100 nm TiO_2 (mix of anatase and rutile) and 0.3–1 μm TiO_2 (anatase containing small amount of rutile) (Karlsson *et al.*, 2009). The same anatase TiO_2 nanoparticles and rutile TiO_2 nanoparticles and microparticles used in the present study have recently been tested for cytotoxicity and genotoxicity in a human bronchial epithelial cell line (BEAS 2B) (Falck *et al.*, 2009). Based on their capacity to reduce BEAS2B viability after 24, 48, and 72 h, as assessed by the Trypan Blue assay, the particles were ranked as follows: rutile micro > anatase nano > rutile nano. We obtained a different ranking for cytotoxicity results in SHE (rutile nano = anatase nano > rutile micro), confirming the importance of the method and the model used for cytotoxicity assessment.

Cytotoxic activity of metal oxide particles is often associated with an increase in intracellular ROS (Nel *et al.*, 2006). In this study, TiO_2 nanoparticles and microparticles were shown to increase ROS contents in SHE, with anatase nanoparticles being the most active. For iron oxides, a moderate effect was only observed with Fe_2O_3 nanoparticles, consistent with the lower cytotoxic potential of iron oxides compared to TiO_2 particles. At the same mass dose, only anatase TiO_2 and Fe_2O_3 nanoparticles induced more intracellular ROS than their micrometer counterparts. Consequently, the intracellular ROS activity profiles of particles did not correspond exactly to their intrinsic ROS activity. As suggested elsewhere, intracellular ROS may result from both particle surface activity and from the cellular response induced by particle uptake (Xia *et al.*, 2006).

The genotoxic properties of TiO_2 particles did not correspond to their cytotoxicity profiles. In the comet assay, DNA damage was observed for all TiO_2 except rutile nanoparticles. Anatase TiO_2 nanoparticles and microparticles induced the same level of damage. As suggested in previous studies (Gurr *et al.*, 2005; Karlsson *et al.*, 2008), DNA damage induced by TiO_2 particles may be explained by intracellular ROS production. The capacity of TiO_2 nanoparticles or microparticles to induce DNA damage has already been reported in various cell lines. In particular, Gurr *et al.* (2005) examined the induction of comet after 1-h treatment with TiO_2 particles of different size in BEAS2B cells. Assays performed with formamidopyrimidine–DNA glycosylase (FPG), which reveals oxidative DNA damage, showed significant effect after treatment with 10 nm (Hombikat UV100), 20 nm anatase TiO_2 (Millenium PC500), and 200 nm rutile TiO_2 (Kanto Chemical) but not with anatase TiO_2 of 200 nm (Kanto Chemical) and anatase TiO_2 >200 nm (Sigma-Aldrich). Interestingly, in the absence of FPG, similar levels of

Table 3. Summary of acellular and cellular effects of particles.

Particles	Intrinsic ROS (with H_2O_2)	Cytotoxicity	Intracellular ROS	DNA damage	Micronucleus formation
TiO_2 A nano	++	++++	++	+	−
TiO_2 A micro	+	+++	+	+	−
TiO_2 R nano	++	++++	+	−	−
TiO_2 R micro	+	+++	+	+	−
TiO_2 P25	++	++++	+	+	−
Fe_3O_4 nano	++	+	−	−	−
Fe_3O_4 micro	+	+	−	−	−
Fe_2O_3 nano	++	++	+	−	−
Fe_2O_3 micro	+	+	−	−	−

DNA damage were observed for all particles, independent of their size. Falck *et al.* (2009) also performed comet assays without FPG in BEAS2B exposed to TiO_2 particles identical to ours for 24, 48, and 72 h. In agreement with our results, they concluded that anatase TiO_2 nanoparticles and rutile TiO_2 microparticles induced more DNA damage than rutile TiO_2 nanoparticles. Concerning iron oxide particles, Karlsson *et al.* (2009) observed no clear difference in DNA damage in A549 exposed for 4 h to different-sized Fe_2O_3 and Fe_3O_4 particles.

In our study, no chromosomal damage was detected in the micronucleus assays for any of the TiO_2 and iron oxide nanoparticles or microparticles. To our knowledge, there is no published data regarding the micronucleus-inducing effects of Fe_2O_3 and Fe_3O_4 particles. However, the capacity of TiO_2 nanoparticles to produce chromosomal damage has previously been demonstrated in different cell lines with particle samples from different sources. In relation to size–effects, Rahman *et al.* (2002) showed that 20-nm size but not 200-nm size TiO_2 particles at 1 μg cm^{-2} (crystal phase not given) were able to induce micronuclei in SHE cells after 12, 24, 48, 66, and 72 h. In contrast, Gurr *et al.* (2005) showed that anatase TiO_2 of both 10 and 200 nm size (10 μg mL^{-1}) induced significant micronuclei formation in BEAS2B after 24 h. In the study of Falck *et al.* (2009), only anatase TiO_2 nanoparticles (with the same origin as ours) induced minor micronucleus formation at 10 and 60 μg cm^{-2} in BEAS2B after 72 h without a clear dose–effect.

CONCLUSIONS

The results of this study are summarized in Table 3. When compared to microparticles, specific 'nanosize effects' of nanoparticles were observed: their ability to generate intrinsic ROS (for all TiO_2 and iron oxide particles in the presence of H_2O_2), to induce cytotoxicity (except Fe_3O_4) and, for anatase TiO_2 and Fe_2O_3, to induce intracellular ROS. The absence of a correlation between the cytotoxicity of particles and their BET SSA (except for Fe_2O_3) suggests that the BET SSA does not represent the biologically active surface of particles that are mainly present in the form of microsized agglomerates in the culture medium. Genotoxicity results for all metal oxide particles indicated the absence of a nanosize effect. In agreement with a previous review on the genotoxic effects of nanoparticles (Landsiedel *et al.*, 2009), we suggest that *in vitro* cytotoxicity and genotoxicity induced by metal oxide nanoparticles are not always higher than those induced by their bulk counterparts. This work illustrates the difficulty in assessing the toxicological effect of nanoparticles compared to their microsized counterparts because industrial processes are different for nanoparticles and microparticles and generally produce chemical and physical changes other than size reduction. Ideally, particles used in future size comparison studies (nano versus microparticles) should be specifically synthesized and designed for this purpose, with a high degree of homology in chemical composition, crystal phase, shape, and purity.

REFERENCES

Allouni ZE, Cimpan MR, Hol PJ *et al.* (2009) Agglomeration and sedimentation of TiO2 nanoparticles in cell culture medium. Colloids Surf B Biointerfaces; 68: 83–7.

Arenz M, Mayrhofer KJ, Stamenkovic V *et al.* (2005) The effect of the particle size on the kinetics of CO electrooxidation on high surface area Pt catalysts. J Am Chem Soc; 127: 6819–29.

Auffan M, Rose J, Bottero JY *et al.* (2009a) Towards a definition of inorganic nanoparticles from an environmental, health and safety perspective. Nat Nanotechnol; 4: 634–41.

Auffan M, Rose J, Wiesner MR *et al*. (2009b) Chemical stability of metallic nanoparticles: a parameter controlling their potential cellular toxicity in vitro. Environ Pollut; 157: 1127–33.

Bermudez E, Mangum JB, Wong BA *et al*. (2004) Pulmonary responses of mice, rats, and hamsters to subchronic inhalation of ultrafine titanium dioxide particles. Toxicol Sci; 77: 347–57.

Bhattacharya K, Davoren M, Boertz J *et al*. (2009) Titanium dioxide nanoparticles induce oxidative stress and DNA-adduct formation but not DNA-breakage in human lung cells. Part Fibre Toxicol; 6: 17.

Brunauer S, Emmet PH, Teller E. (1938) Adsorption of gases in multimolecular layers. J Am Chem Soc; 60: 309–19.

Cohn CA, Simon SR, Schoonen MA. (2008) Comparison of fluorescence-based techniques for the quantification of particle-induced hydroxyl radicals. Part Fibre Toxicol; 5: 2.

Collins AR, Gedik CM, Olmedilla B *et al*. (1998) Oxidative DNA damage measured in human lymphocytes: large differences between sexes and between countries, and correlations with heart disease mortality rates. FASEB J; 12: 1397–400.

EC. (2011) European Commission: Commission recommendation on the definition of nanomaterial (draft). Brussels, Belgium: European Commission.

Falck GC, Lindberg HK, Suhonen S *et al*. (2009) Genotoxic effects of nanosized and fine TiO2. Hum ExpToxicol; 28: 339–52.

Fenoglio I, Greco G, Livraghi S *et al*. (2009) Non-UV-induced radical reactions at the surface of TiO2 nanoparticles that may trigger toxic responses. Chemistry; 15: 4614–21.

Gurr JR, Wang AS, Chen CH *et al*. (2005) Ultrafine titanium dioxide particles in the absence of photoactivation can induce oxidative damage to human bronchial epithelial cells. Toxicology; 213: 66–73.

Hood E. (2004) Nanotechnology: looking as we leap. Environ Health Perspect; 112: A740–9.

Hussain SM, Hess KL, Gearhart JM *et al*. (2005) In vitro toxicity of nanoparticles in BRL 3A rat liver cells. Toxicol In Vitro; 19: 975–83.

IARC. (2010) Carbon black, titanium dioxide, and talc. In IARC Monographs on the Evaluation of Carcinogenic Risks to Humans. Lyon, France: World Health Organization, International Agency for Research on Cancer. 93: 1–452.

ISO. (2008) Particle size analysis—dynamic light scattering (DLS). Geneva, Switzerland: ISO 22412:2008; p. 17.

Jeng HA, Swanson J. (2006) Toxicity of metal oxide nanoparticles in mammalian cells. J Environ Sci Health A Tox Hazard Subst Environ Eng; 41: 2699–711.

Karlsson HL, Cronholm P, Gustafsson J *et al*. (2008) Copper oxide nanoparticles are highly toxic: a comparison between metal oxide nanoparticles and carbon nanotubes. Chem Res Toxicol; 21: 1726–32.

Karlsson HL, Gustafsson J, Cronholm P *et al*. (2009) Size-dependent toxicity of metal oxide particles—a comparison between nano- and micrometer size. Toxicol Lett; 188: 112–8.

Kato H, Suzuki M, Fujita K *et al*. (2009) Reliable size determination of nanoparticles using dynamic light scattering method for in vitro toxicology assessment. Toxicol In Vitro; 23: 927–34.

Landsiedel R, Kapp MD, Schulz M *et al*. (2009) Genotoxicity investigations on nanomaterials: methods, preparation and characterization of test material, potential artifacts and limitations—many questions, some answers. Mutat Res; 681: 241–58.

LeBel CP, Ischiropoulos H, Bondy SC. (1992) Evaluation of the probe 2′,7′-dichlorofluorescin as an indicator of reactive oxygen species formation and oxidative stress. Chem Res Toxicol; 5: 227–31.

Liu SY, Long L, Yuan Z *et al*. (2009) Effect and intracellular uptake of pure magnetic Fe3O4 nanoparticles in the cells and organs of lung and liver. Chin Med J (Engl); 122: 1821–25.

Nel A, Xia T, Madler L *et al*. (2006) Toxic potential of materials at the nanolevel. Science (New York, NY); 311: 622–7.

Oberdorster G, Ferin J, Finkelstein G *et al*. (1990) Increased pulmonary toxicity of ultrafine particles? II. Lung lavage studies. J Aerosol Sci; 21: 384–7.

Oberdorster G, Ferin J, Gelein R *et al*. (1992) Role of the alveolar macrophage in lung injury: studies with ultrafine particles. Environ Health Perspect; 97: 193–9.

Oberdorster G, Oberdorster E, Oberdorster J. (2005) Nanotoxicology: an emerging discipline evolving from studies of ultrafine particles. Environ Health Perspect; 113: 823–39.

OECD. (2010) OECD 487 Guideline for testing of chemicals, in vitro mammalian cell micronucleus test. Paris, France: Organisation for Economic Co-operation and Development. p. 23.

Pant K, Aardema MJ. (2008) The Syrian hamster embryo (SHE) low pH cell transformation assay. Curr Protoc Toxicol; 35: 20.23.21–20.23.16.

Rahman Q, Lohani M, Dopp E *et al*. (2002) Evidence that ultrafine titanium dioxide induces micronuclei and apoptosis in Syrian hamster embryo fibroblasts. Environ Health Perspect; 110: 797–800.

Savolainen K, Alenius H, Norppa H *et al*. (2010) Risk assessment of engineered nanomaterials and nanotechnologies—a review. Toxicology; 269: 92–104.

Schulze Isfort C, Rochnia M. (2009) Production and physicochemical characterisation of nanoparticles. Toxicol Lett; 186: 148–51.

Sclafani A, Herrmann JM. (1996) Comparaison of the photoelectronic and photocatalytic activities of various anatase and rutile forms of titania in pure liquid organic phases and in aqueous solution. J Phys Chem; 100: 13655–61.

Setsukinai K, Urano Y, Kakinuma K *et al*. (2003) Development of novel fluorescence probes that can reliably detect reactive oxygen species and distinguish specific species. J Biol Chem; 278: 3170–5.

Soto K, Garza KM, Murr LE. (2007) Cytotoxic effects of aggregated nanomaterials. Acta Biomater; 3: 351–8.

Wang JJ, Sanderson BJ, Wang H. (2007) Cyto- and genotoxicity of ultrafine TiO2 particles in cultured human lymphoblastoid cells. Mutat Res; 628: 99–106.

Warheit DB, Webb TR, Reed KL *et al*. (2007) Pulmonary toxicity study in rats with three forms of ultrafine-TiO2 particles: differential responses related to surface properties. Toxicology; 230: 90–104.

Xia T, Kovochich M, Brant J *et al*. (2006) Comparison of the abilities of ambient and manufactured nanoparticles to induce cellular toxicity according to an oxidative stress paradigm. Nano Lett; 6: 1794–807.

Zhu MT, Feng WY, Wang B *et al*. (2008) Comparative study of pulmonary responses to nano- and submicron-sized ferric oxide in rats. Toxicology; 247: 102–111.